PERGAMON

Available online at www.sciencedirect.com

SCIENCE DIRECT®

International Journal of Multiphase Flow 29 (2003) 195–217

International Journal of Multiphase Flow

www.elsevier.com/locate/ijmulflow

Gas–droplet turbulent velocity correlations and two-phase interaction in an axisymmetric jet laden with partly responsive droplets

V. Ferrand, R. Bazile *, J. Borée, G. Charnay

Institut de Mécanique des Fluides de Toulouse, UMR CNRS/INPT-UPS 5502, Av. Camille Soula, 31400 Toulouse, France

Received 25 March 2002; received in revised form 5 November 2002

Abstract

The effect of fluid–particle interaction on the development of an axisymmetric jet laden with partly responsive droplets is discussed in this paper. Measurements up to 40 diameters were obtained by using phase Doppler and laser induced fluorescence technique (combining both techniques provides the mass concentration of liquid per size class).

Comparison of the mean gas velocity fields with and without drops shows clearly the expected effects of the dispersed phase on the carrier phase, known as "two way coupling".

Statistics of the velocity of the fluid "seen" by the particles have been calculated after temporal reconstruction of the turbulent signal of the continuous phase. The fluid–particle correlations are presented and used to analyse the radial evolution of the particle stresses. We show that the anisotropy of the drop fluctuation motion is large and associated with production mechanisms, via interaction with mean particle velocity gradients.

Finally the attenuation term, which complements the conventional transport equation of the turbulent kinetic energy for single-phase flow, is calculated. Radial profiles are presented ($X = 20d_0$) and compared with an estimation usually found in the literature, when neglecting the fluid–particle correlations. The results clearly show that such estimation really overestimates the magnitude of the term responsible for the direct turbulence attenuation by the particles.

Keywords: Droplet-laden jet; Fluid–particle velocity correlations; Turbulence modulation; Two-way coupling; Phase Doppler anemometer; Planar laser induced fluorescence

* Corresponding author.
E-mail address: bazile@imft.fr (R. Bazile).

0301-9322/03/$ - see front matter
PII: S0301-9322(02)00151-9

1. Introduction

The important role played by sprays in combustion (internal combustion engines, burners, rocket engines, etc.) offers challenges for the development and application of laser diagnostics in two-phase flows. Sprays of small droplets are a matter for research concerning turbulent, dense two-phase jets, where the mechanisms of interaction between the air and drops are still not well understood.

We are interested in flows where the volume fraction α of the dispersed phase is small enough to assure that dispersion is governed by the turbulent flow (i.e. particle/particle collisions are neglected). However, the droplet mass-loading ratio $\phi = \dot{m}_L/\dot{m}_G$ (where $\dot{m}_L$ and $\dot{m}_G$ represent the liquid and gas mass flow rates respectively) is large enough to introduce significant mean and turbulent energy exchanges between the phases, known as "two-way coupling". Therefore, accurate measurements of such effects are essential for the development of recent two-phase flow modeling (Crowe, 2000) and for a good prediction of dense spray behaviour.

A large number of recent studies focus on modeling the turbulence attenuation by the dispersed phase. Yuan and Michaelides (1992), Yarin and Hetsroni (1994), Kenning and Crowe (1997) proposed physical models to explain experimental observations, while the traditional approach for modeling particle-laden flows is based on extension of Reynolds-averaged Navier–Stokes equations used for single-phase flows (Elghobashi and Abou-Arab, 1983; Kulick et al., 1994; Squires and Eaton, 1990; Simonin et al., 1995; Sommerfeld, 1993; Berlemont et al., 1995). In two-phase flows, turbulent quantities, such as kinetic energy and dissipation, are modified directly by the dispersed phase through the interfacial momentum transfer. To take this transfer into account, extra sources/sink terms are added to the transport equations. Turbulent kinetic energy transport equation can then be expressed as:

$$\frac{D\langle u_{G,i}u_{G,i}\rangle}{Dt} = P_{G,ii} + T_{G,ii} - \varepsilon + \Pi_{G,ii} \tag{1.1}$$

$u_{G,i}$ is the fluctuating component of the gas phase velocity on the direction i and $\langle\cdot\rangle$ is the Reynolds average operator. $P_{G,ii}$, $T_{G,ii}$ and ε denote respectively the conventional production, transport and dissipation of turbulent kinetic energy as expressed for single-phase flows. One can note that these terms can be modified indirectly by the presence of the dispersed phase through a modification of turbulence dynamics itself. The extra source/sink term, $\Pi_{G,ii}$, due to a 'direct interaction' of the particles with the surrounding fluid, is given by the work applied by the particles to the surrounding fluid:

$$\Pi_{G,ii} = -\frac{2}{\rho_G}\langle u_{G,i}F_{r,i}\rangle \tag{1.2}$$

Note that here the gas volume fraction is kept to unity ($\alpha_G \approx 1$) since the liquid volume fraction is negligible everywhere ($\alpha \ll \alpha_G$). $F_{r,i}$ represents the instantaneous force per unit volume acting on droplets (or particles). For heavy droplets ($\rho_L \gg \rho_G$), this force reduces to the drag force contribution, $F_{r,i} = C_d(3\alpha_d\rho_G)/4D(U_{G,i} - U_{d,i})|U_{G,i} - U_{d,i}| = (\alpha_d\rho_L)/\tau_d(U_{G,i} - U_{d,i})$. C_d is the drag coefficient determined from the correlation: $C_d = 24/\mathrm{Re}_p$, α_d is the volume fraction of the size class d and τ_d is the droplet relaxation time. $U_{G,i}$ and $U_{d,i}$ represent respectively the instantaneous gas and droplets velocity. It follows:

$$\langle u_{G,i}F_{r,i}\rangle = \frac{\langle Cm_d\rangle}{\tau_d}\langle u_{G,i}(U_{G,i} - U_{d,i})\rangle \tag{1.3}$$

where Cm_d is the instantaneous droplet concentration $\langle Cm_d\rangle = \alpha_d\rho_L$. Developing the expression (1.3), it follows that the closure of $\Pi_{G,ii}$ requires the specification of the correlation between the velocity of the droplets and the velocity of the surrounding fluid. Therefore, the modeling of the gas/droplet turbulent velocity correlations $\langle u_{G,i}u_{d,i}\rangle$ (written also $\langle u_{G,i}u_{d,i}\rangle_d$ to underline the average on the dispersed elements) appears to be a crucial stage to predict correctly the coupling between the two phases, independently of the approach retained to describe the dispersed phase, whether Lagrangian or Eulerian (Squires and Eaton, 1990; Simonin, 2000).

When partly responsive particles are concerned, it is clearly not possible to neglect the influence of fluid–particle correlations (as supposed by Kulick et al., 1994) that contribute to reduce the magnitude of $\Pi_{G,ii}$. However, very little is known about these quantities due to the difficulty of measuring particle velocity and gas velocity in the vicinity of the particle.

As experiment is concerned, Sakakibara et al. (1996) developed a particle image velocimetry system which allows discrimination of large particles from the seeding and gives simultaneously access to particle and gas velocities. This method, based on the scattered light intensity is however restricted to particles larger than 40 μm and to dilute two-phase flows, since the images of particles (that appear to be as large as 10 times their real sizes) should not overlap. Longmire et al. (1999) developed a similar technique based on tracking of solid particles.

The phase Doppler anemometer, particularly well adapted to two-phase flows characterization, can provide temporal correlations of fluid–particle velocities (Hädrich and Erdmann, 1998) but, since it is a single particle counter, it does not provide the appropriate correlations for zero time delay needed for the models. Prévost et al. (1996) proposed a method to reconstruct the temporal velocity of the gas phase of a dilute two-phase jet by interpolating the signal of the fluid tracers. The instantaneous fluid velocity surrounding each particle (the fluid velocity "seen" by the particles) was obtained thanks to that reconstruction. The fluid–particle correlations $\langle u_G u_d\rangle_d$ were then calculated.

The objectives of the present work are to extend and adapt the method introduced by Prévost et al. (1996) to analyze a more concentrated jet where the fluid–particle correlations are expected to contribute actively to the magnitude of the turbulence modulation. The experimental configuration is an axisymmetric, turbulent, two-phase jet, where the boundary conditions for air and drops are well controlled. The exit Reynolds number is 9500, the initial liquid mass loading is $\phi = 0.73$ for a droplet-size range of 1–110 μm. This wide range of droplet diameters (i.e. Stokes number) is essential to account for the various behaviours of the gas-droplet correlations, from the droplets that perfectly follow the fluid to those unresponsive to any gas fluctuations.

Section 2 presents the experimental configuration and the associated phase Doppler and laser induced fluorescence (PLIF) measurement techniques applied to the round jet. Main characteristics of the two-phase flow are described and the effects of droplets on the mean gaseous flow are underlined by comparing the gas phase behaviour to a single-phase jet. Section 3 is dedicated to the fluid–particles turbulent velocity correlations. The measurement approach, based on the reconstruction of the instantaneous gas velocity, is described and validated on the well-characterized two-phase round jet. Results are analyzed in term of Stokes number. A specific measurement method (Ferrand et al., 2001) is used to access to the mean value of the local concentration per

size class $\langle Cm_d \rangle = \alpha_d \rho_L$, where α_d is directly used to characterize turbulence interaction in the Eulerian approach (see Section 4). The turbulent coupling terms $\Pi_{G,ij}$ are evaluated for the normal and shear Reynolds stresses in Section 4. The major contribution of the gas-droplet correlations on these coupling terms is then clearly demonstrated.

2. Experimental configuration and flow properties

2.1. Generation of the droplet-laden jet

The experimental set-up is shown in Fig. 1. The two-phase jet emerges from a convergent nozzle with an exit diameter (d_0) of 8 mm. The air passes through a mass flowmeter to ensure a constant flow rate of 53.4 l/min corresponding to a mean air exit velocity of 18 m/s. The Reynolds number at the exit, based on d_0, is 9.500.

Four air-assisted injectors produce drops in the diameter range 1–110 μm. All of the 53.4 l/min of air flow passes through the air blast atomizers. The liquid is a solvent ($\rho_L = 760$ kg/m^3), whose material properties (surface tension, density) are close to those of gasoline. Particular effort has been expended to find the convergent shape of the nozzle. The walls have been drawn according to a 5° polynomial with first and second derivatives infinite at the top and the bottom sections (see Fig. 1b). This shape ensures good flow aerodynamics and controls the liquid film formation, caused by droplet impacts on the wall.

A simple collector device is added at the jet nozzle exit, to trap and drain off the liquid film. The mass flow rate of the trapped liquid film is measured by a weighing technique and subtracted from

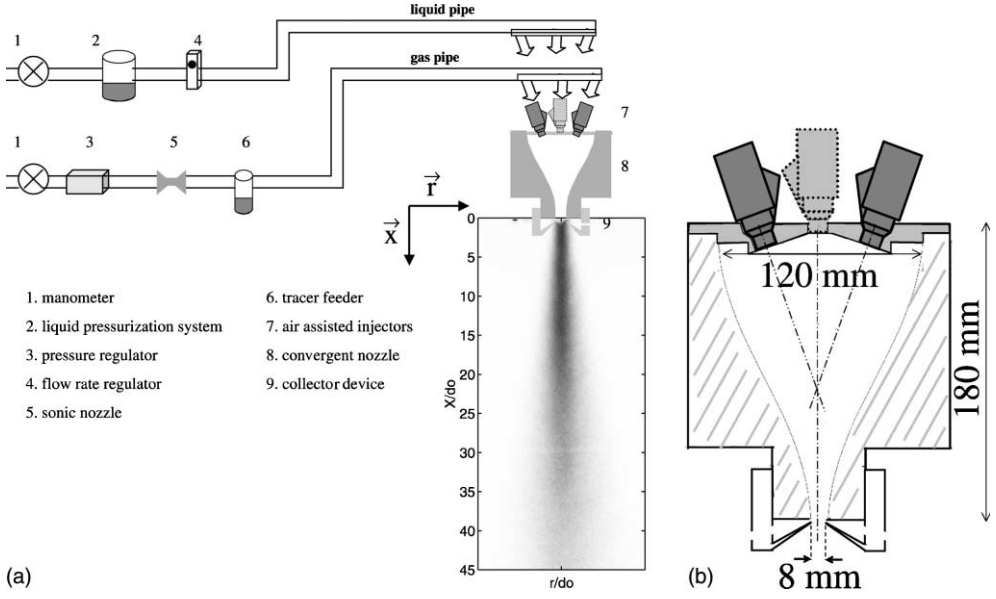

Fig. 1. (a) Experimental set-up, (b) Drawing of the nozzle: the contraction ratio and the length of the nozzle profile are respectively equal to 15 and 180 mm.

the total liquid mass flow rate, yielding the initial mass loading ratio $\phi = \dot{m}_L/\dot{m}_G = 0.73 \pm 4\%$ (liquid to gas exit mass flow rate ratio). The vertical jet discharges into a cubic chamber (0.5 m × 0.5 m × 0.5 m). The experimental set-up is mounted on a three-axis displacement table, allowing vertical measurements from $X = 2.5d_0$ to $40d_0$.

The jet is described by a cylindrical coordinate system (X, r, θ) to indicate the axial, radial and azimuthal directions, while the components of the mean and fluctuating velocity fields are denoted by $(U, V, W = 0)$ and (u, v, w) respectively. Subscript "0" indicates the exit properties and subscript "c" indicates the centerline properties. Subscripts "G" and "d" indicate gas and droplets properties respectively.

2.2. Phase Doppler and PLIF set-up

Two different laser diagnostics are applied to characterise the jet. A two component phase Doppler system is used to simultaneously measure droplet velocities and diameters, while PLIF technique is dedicated to the measurement of the instantaneous liquid concentration fields.

A new method that coupled these two measurement techniques was developed to reach the mean value of the local mass concentration, $\langle Cm_d \rangle$, of each class of drops. This term, crucial to characterise the dispersion of the drops as well as the energy transfer between the phases (see Eqs. (4.1)–(4.3)) cannot be calculated from standard phase Doppler data for the strong concentrations studied in the present work (Qiu and Sommerfeld, 1992). The following paragraph describes the main characteristics of the phase Doppler and PLIF set-up. The bases and the validation of the method of coupling can be found in (Ferrand et al., 2001).

A two-components laser phase Doppler system (Dantec) was used. The beam emitted from an Argon laser is divided into two beams of wavelengths $\lambda_1 = 514.5$ nm and $\lambda_2 = 488$ nm for two-component velocity measurements. The measurement volume is 240 μm long (the projected PM slit width is 100 μm) with a diameter and fringe spacing of 150, 4.2 and 142 μm, 3.8 μm for the streamwise and the transverse direction respectively. The receiving optics is placed 32° to the forward scatter direction, to minimize the contribution of reflected light. Doppler bursts are processed by the Dantec 58N80 phase Doppler Signal Processor. All data are transferred to a PC before being post-processed by customized Matlab programs. A single measurement at a given point generally comprises 20,000 droplets. Seven radial profiles ($X = 2.5d_0$–$40d_0$) and the centreline profile are measured. The behaviour of the liquid dispersion is analysed by dividing the drops into size classes 5–10, 10–20, 20–30 and 90–100 μm. The gas velocity is obtained by averaging the velocity measurements in the size class 0–5 μm, droplets of this size class have been verified to be good tracers for the gaseous phase (Section 2.3). Moreover, very small oil droplets of about 2 μm are added to the air pipe to seed the air jet. When the seeding in the chamber is dense, multiple scattering disturbs the signals emitted by the drops contained in the jet and introduces errors in the measurements of sizes. For this reason the tracers are only introduced in the jet nozzle. Only a small amount of seeding recirculates in the chamber and a correction for the well-known bias due to the "condition seeding" is applied (see Section 3.1).

The PLIF imaging technique is based on the UV planar laser-induced fluorescence. The pulsed beam ($\lambda = 266$ nm, $\Delta t = 10$ ns, $I_0 = 40$ mJ, $f = 10$ Hz) provided by the fourth harmonic of a Nd:Yag laser is focused into a vertical light sheet (20 cm height, 300 μm thick), passing through the axis of the jet. Fluorescence emission scattered by the drops is imaged at 90° onto a gated

intensified CCD camera (PCO Sensicam, 12-bit numeric, 1280 × 1024 pixels) with a 58 mm-$F/1.2$ objective lens. The camera is equipped with a pass-band filter BG 25 that rejects contributions at the laser wavelength (Mie scattering, reflection...). With a camera located 30 cm from the laser sheet, the magnification is about 0.2. Despite the high dynamic range of the camera (12 bits), the imaging system cannot completely cover the range of drop diameters, since the scattered intensities scale as D^3. With the present imaging system, the threshold of detection is reached for a probed mass of liquid corresponding to that of a 15 μm droplet alone in the measurement volume (440 μm × 440 μm × 300 μm). Statistically, this drastic condition is very improbable in the dense region and fluorescence images provide reliable data, even though the mass contribution of the smallest droplets remains a little bit underestimated. The video signal is stored in real time in a PC before being post-processed with Matlab programs. The processing and the accuracy of the liquid concentration measurement (estimated at ±6%), which are not the main subject here, are discussed in a previous paper (Ferrand et al., 2001).

2.3. Two-phase flow main characteristics

2.3.1. Liquid phase characteristics

The initial droplet size distribution is displayed in Fig. 2 for the centerline of the jet ($r = 0$). The corresponding number average and mass average diameters are $D_{30} = 20$ μm and $D_{10} = 60$ μm, respectively. All effects resulting in a modification of droplet size, such as secondary break-up effects, vaporization or coalescence due to collisions have been analyzed in (Ferrand, 2001) and are negligible. Furthermore, the mass flow rate of each size class (evaluated with the phase Doppler/PLIF coupling method) was verified to be constant along the measurement area (Ferrand et al., 2001). In consequence, we can consider that all droplets keep a constant diameter D during their motion in the current flow.

In a turbulent flow, droplet motion is directly connected to the ability of the droplet to respond to the large turbulent structures of the jet (Longmire and Eaton, 1992). The Stokes number, St, is defined as the ratio of the droplet aerodynamic time constant τ_d to an appropriate turbulent time scale τ_t. τ_t is chosen as the ratio of a large eddy length scale $L_{1/2}$ (the half width of the jet, esti-

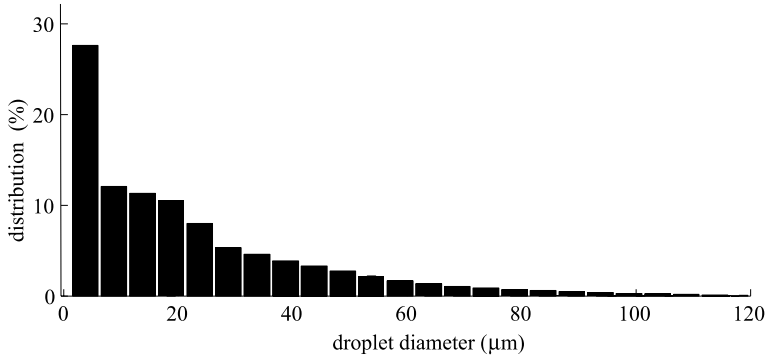

Fig. 2. Histogram of diameters of drops ($X = 2.5d_0$, $r = 0$).

mated from mean velocity profile) to the standard deviation of the centerline fluctuating velocity, $\sqrt{\langle u_G u_G \rangle_c}$:

$$\tau_t = L_{1/2}(X)/\sqrt{\langle u_G u_G \rangle_c}$$

τ_d is defined by

$$\tau_d = \frac{4D\rho_L}{3C_D|U_G - U_L|\rho_G} \tag{2.1}$$

where C_D is the drag coefficient. A Stokes number of order of one separates the drops, which follow the fluctuations of the fluid ($St \ll 1$), from those that are unresponsive to any fluctuations ($St \gg 1$). Droplets in the size class 0–5 μm present a Stokes number ranging from 0.03 at the jet exit to less than 0.002 in the far field of the jet (Fig. 3). These droplets, able to follow the smallest turbulent scales (Ferrand, 2001) will constitute good tracers for the continuous phase. The decrease in the Stokes number, when going far from the nozzle exit is due to the continuous increase of τ_t (proportional to X^2). So far, one can note that all droplets become at least partially responsive to gaseous fluctuations downstream of $20d_0$. The fact of working with a wide range of partially responsive drops appears of first interest to analyse the gas–droplet turbulent velocity correlations. These correlations are expected to be negligible for the big drops ($St \gg 1$). On the contrary they are equivalent to the fluid Reynolds stress for the smallest droplets (tracers of the gas phase, $St \ll 1$). An intermediate behaviour depending on the size class is expected for partially responsive drops.

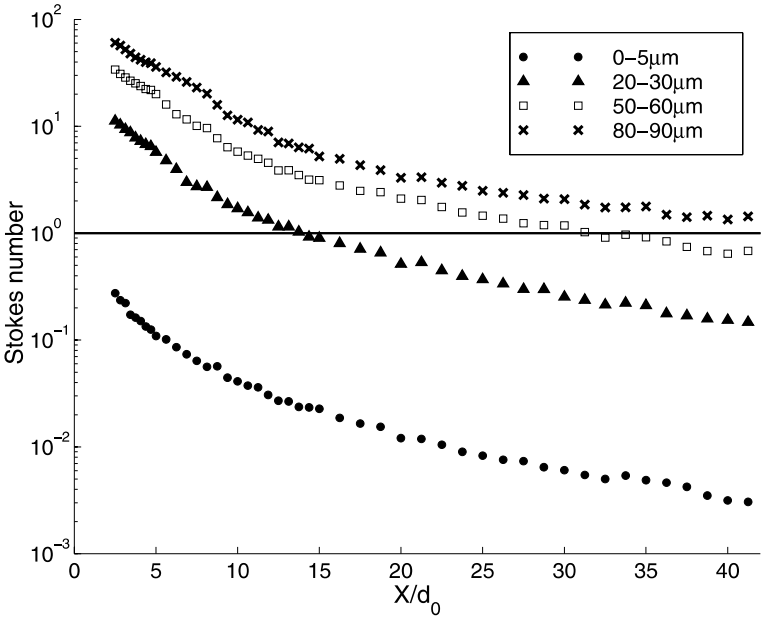

Fig. 3. Longitudinal evolution of the Stokes number of for different droplet size classes ($X = 20d_0$).

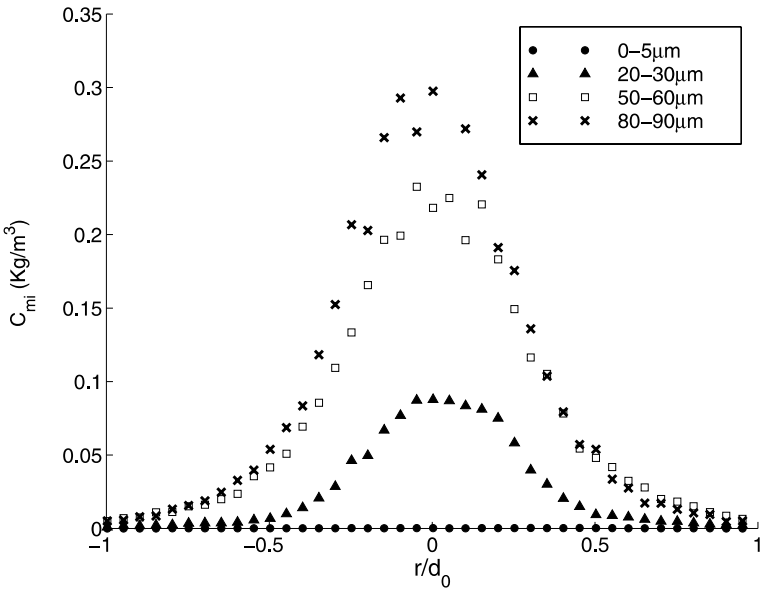

Fig. 4. Radial profile of the initial mass concentration of the different droplet size classes ($X = 2.5d_0$).

Radial profiles of the initial mass concentration ($X = 2.5d_0$) corresponding to four different size classes are presented in Fig. 4. The precision of measurements has been estimated at 7% (Ferrand et al., 2001). Whereas the concentration of each class seems to be weak, the cumulated concentration of all the size classes present in the flow reaches 2.2 kg/m^3 in the central zone of the jet. This value of the total liquid concentration, directly provided by PLIF measurements, corresponds to a volume fraction of the dispersed phase ($\alpha = 2.2/\rho_L$) of 0.3%. For such volume fractions, it is well known that the dispersed phase can induce significant modifications of the carrier phase by exchange of averaged and turbulent momentum. Particle inertia and mass loading are the crucial parameters that control the mean and turbulent momentum exchange between the phases. To analyze the effect of liquid concentration on gas properties, the continuous phase of the two-phase case $\phi = 0.73$ is compared to the single-phase jet $\phi = 0$, with equivalent exit Reynolds number.

2.3.2. Liquid and gas phases interaction: two-way coupling

Mean gaseous velocity fields given by the phase Doppler measurements for the cases $\phi = 0$ and $\phi = 0.73$ are presented in Fig. 5a and b respectively. Quantitative information are displayed in Table 1. The main effects of the liquid phase are the increase in the centerline mean gas velocity and the decrease in the spreading rate of the jet (−26% compared to the single-phase jet, see Table 1). These observations are in agreement with previous experimental studies on particle-laden jets (Modaress et al., 1983; Fleckhauss et al., 1987; Hardalupas et al., 1989; Mostafa and Mongia, 1988).

One can note that the slope ($k = 0.205$) of the linear curve fitting the inverse of the axial velocity of the single-phase jet velocity $(U_0/U)_c$ (see Table 1 and Fig. 6a), is comparable with previous studies on single-phase round jets (Wygnanski and Fielder, 1969) and is about twice the slope

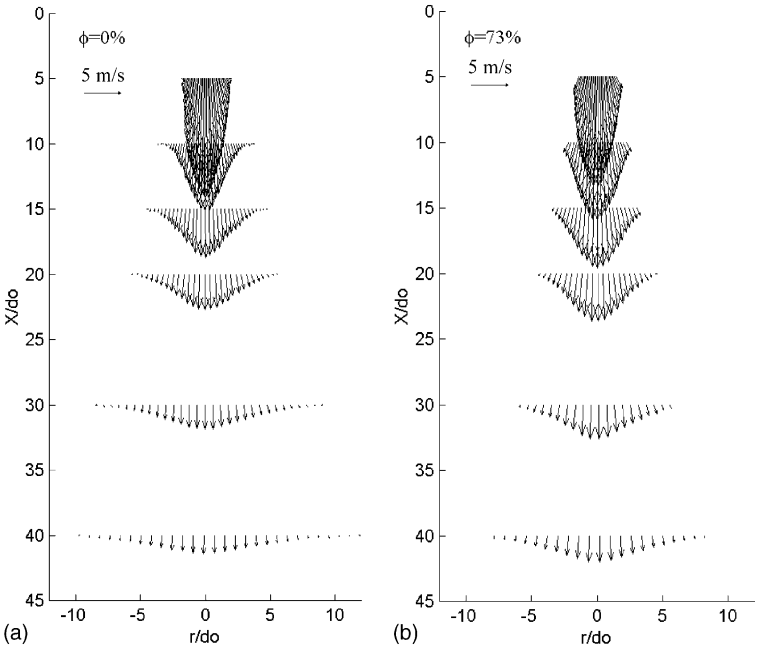

Fig. 5. Mean gas velocity field obtained from phase Doppler measurements: (a) single-phase jet ($\phi = 0$); (b) two-phase jet ($\phi = 0.73$).

Table 1
Penetration and spreading of the single-phase and two-phase jet

	Single-phase jet $\phi = 0$	Two-phase jet $\phi = 0.73$
Mean velocity centerline decrease $\frac{(U_{GC})_0}{U_{GC}(X)} = \frac{k}{d_0}(X - X_0)$	$k = 0.205$	$k = 0.12$
Half-jet width $\frac{U_G(L_{1/2}, X)}{U_{GC}(X)} = \frac{1}{2}$	$L_{1/2} = 0.105X$	$L_{1/2} = 0.078X$

obtained for the two-phase jet $\phi = 0.73$. It has been shown that this longitudinal mean velocity increase results from a combined action of mean momentum transfer from the drops to the airflow and decrease in turbulent diffusion intensity (Ferrand et al., 2001).

The two-way coupling clearly observed here on the mean velocity field cannot be dissociated from modifications that occur on the turbulent field of the carrier phase. In such flows, gas turbulence has been found to be significantly attenuated when droplets are fine enough (Parthasarathy and Faeth, 1990; Yuan and Michaelides, 1992; Sakakibara et al., 1996; Kenning and Crowe, 1997).

Fig. 6b reports the axial evolution of the normalized turbulent kinetic energy $k = 1/2(u_G'^2 + 2v_G'^2)_c$, both for the single-phase case and the two-phase case. These measurements indicate a reduction of the turbulence intensity when droplets are added to the gas flow. Droplets effect is shown to decrease slowly when the distance from the exit increases and the droplet concentration decreases. At the position $X = 20d_0$ (profile more particularly analyzed in Sections

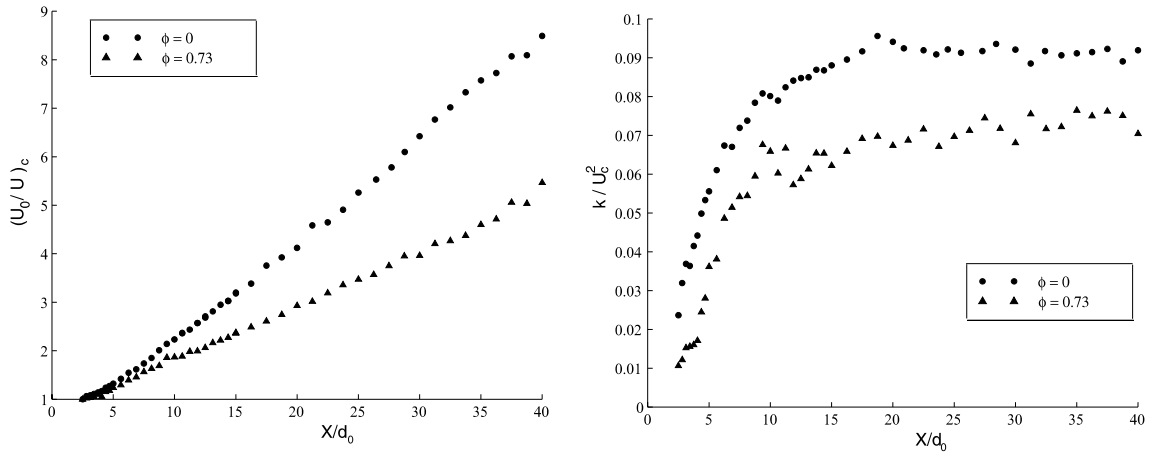

Fig. 6. Centerline evolution of gas properties for the single-phase jet ($\phi = 0$) and the two-phase jet ($\phi = 0.73$): (a) inverse of the mean velocity $(U_0/U)_c$; (b) intensity of the turbulent kinetic energy $(k/U^2)_c$.

3 and 4), the dispersed phase induces a reduction in turbulence intensity of 19% compared to the single-phase jet.

Two-way coupling is then effective in that experiment and we propose to measure the exchanges of turbulent kinetic energy between the two phases. To access this quantity following Eq. (1.3), the gas–droplet turbulent velocity correlations appear to be one of the more critical term to determine from both an experimental (Sakakibara et al., 1996; Prévost et al., 1996; Borée et al., 2001) as for a numerical (Simonin et al., 1995; Février and Simonin, 1998) point of view. Next sections are dedicated to the measurement of these correlations (Section 3) and to their contribution in the two-phase coupling term (Section 4).

3. Measurement of the gas–droplet turbulent velocity correlations

3.1. Measurement methodology

The measurement methodology of the gas–droplet turbulent velocity correlations introduced by Prévost et al. (1996) is based on the temporal reconstruction of the gas phase velocity from the phase Doppler data. The velocity reconstruction is performed by using the method proposed by Veynante and Candel (1988) based on the Shannon interpolation of the non-regularly sampled turbulent signal of the gas phase. Knowing the arrival time of the droplets in the measurement volume, it is then possible to estimate the fluid velocity properties when each droplet crosses the measurement volume. This velocity refers to the fluid velocity "seen" by the droplet, that means the instantaneous fluid velocity surrounding a droplet whose diameter is ideally assumed to be much smaller than the smallest scales of turbulence. Fig. 7 shows a sample of the reconstructed signal of the continuous phase. The velocity of the droplets has been superimposed and the instantaneous velocity of the fluid "seen" by the droplets can be deduced. The mean relative velocity "seen" by the particles $\langle U_G - U_d \rangle_d$, is important to predict accurately the mean interfacial

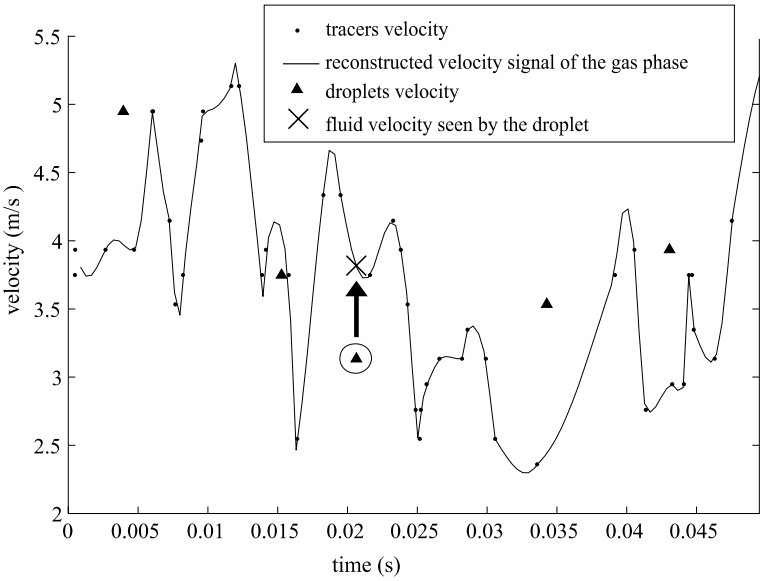

Fig. 7. Temporal evolution of the air velocity and the associated fluid velocities "seen" by the droplets obtained by reconstruction of the phase Doppler signal at $X = 20d_0$ ($r = 0$).

transfers of momentum (Simonin, 1991). This value can be directly calculated from our measurements while models for the corresponding quantities are very important for the numerical predictions of turbulent two-phase flows. In the same way the gas–droplet turbulent velocity correlations "seen by the particles", that appear in the turbulent energy transport equation, are obtained with statistical calculations on each size class.

The measurement accuracy depends directly on the quality of the reconstructed signal of the continuous phase velocity. To assure a correct interpolation of the instantaneous turbulent gas velocity, measurements must be performed with a sufficient data rate when compared to the characteristic frequencies of the turbulent flow. This point becomes particularly critical when working with non-dilute jet such as encountered in the present study. According to the experimental configuration and the instrumentation used, the reconstruction technique was applied at the radial location $X = 20d_0$ to assure an acquisition frequency on the seeding particles larger than 10 times the characteristic frequency of the more energetic eddies ($\mathrm{Fi} = 1/\tau_t \approx 350$ Hz). To reach such a data rate, the jet was seeded with a high density of flow tracers and acquisition parameters (laser power, photomultiplier high voltage) were optimized. Moreover, at this section $X = 20d_0$, all droplets are partly sensitive to gaseous fluctuations ($St \approx \mathrm{O}(1)$, see Fig. 3) and contribute to the kinetic energy exchange between phases.

The convergence statistics of the reconstructed velocities has been checked. In that goal, the energy density spectra have been plotted keeping successively all data of the flow tracers, one out of two and one out of five (Ferrand, 2001), as performed by Prévost et al. (1996). Results were shown to be stable demonstrating the good quality of the air seeding and the capacity for reconstructing correctly the turbulent gas velocity for turbulent frequencies larger than the more energetic ones.

Moreover, to evaluate correctly the fluctuations of the fluid velocity "seen" by the droplets, we have to solve the different turbulent scales that droplets interact with. Each droplet size class is characterized by a relaxation time τ_d (defined by (2.1)). The particle response function to the dragging by the fluid turbulence leads to a filtering effect of the turbulence spectrum. Hinze (1975) showed that the ratio of the particle energy spectra to the fluid energy spectrum is:

$$\frac{E_d(f)}{E_G(f)} = \frac{1}{1 + (2\pi f \tau_d)^2}$$

Fig. 8 represents the reconstructed temporal spectrum of the streamwise turbulent energy $\langle u_G u_G \rangle$. The frequencies f_d pointed in Fig. 7 correspond to a ratio of $E_d/E_G = 0.1$, $(f_d = 3/(2\pi\tau_d))$ indicating the maximum frequencies that droplets can follow. One can observe that the reconstruction method applied here allows to solve the turbulent scales up to these frequencies f_d for the considered size classes 20–30, 50–60 and 80–90 μm.

To evaluate the gas–droplet turbulent velocity correlations, we performed ensemble averaging ranging from 400 samples for the largest size class 80–90 μm to 6000 samples for the 20–30 μm class (see Table 2). The expected statistical errors on the correlations for each size class are

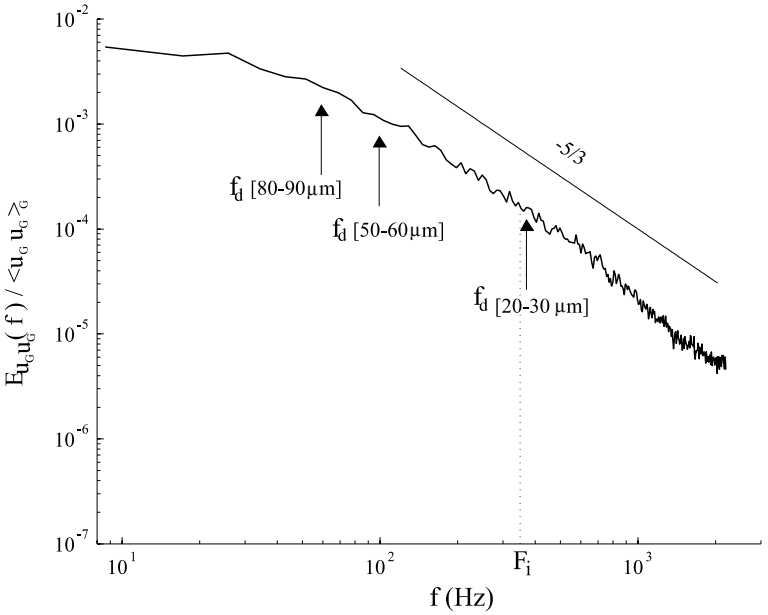

Fig. 8. Energy spectrum relative to the "reconstructed" longitudinal velocity component and the associated "cut of " frequencies f_d for the dispersed phase.

Table 2
Statistical errors estimated for the gas–droplet turbulent correlations for the different size classes

Size class	0–5 μm (gas tracers)	20–30 μm	50–60 μm	80–90 μm
Mean number of samples	35,000	6000	3000	400
Estimated statistical errors	0.8%	1.2%	2.5%	7.3%

reported in Table 2. The size class 80–90 μm appears to be penalized by a lack of samples resulting in statistical errors reaching 7%. Nevertheless, gas–droplet turbulent velocity correlations of the other size classes are obtained with a reasonable accuracy.

3.1.1. Fluid velocity "seen" by the drops, validation of the measurements

We now propose to check the coherence of the results obtained at $X = 20d_0$, by analysing the mean transverse velocity of the fluid ($\widetilde{V}_G$) "seen" by four different size classes of drops. The velocity of the continuous phase, (V_G), is calculated from the corrected data of the size class 0–5 μm.

As the sampling of the tracers in the measurement volume is non-regular, statistics directly carried out on rough data can involve a bias on the velocity measurement (Petrie et al., 1988). Moreover in our configuration, this bias is coupled with the effects of the conditional seeding of the gas phase (see Section 2.2). This conditional seeding is a well-known source of bias in the velocity measurements. Previous experimental studies (Lehman, 1986; Sautet, 1992) showed that the lack of seeding of the surrounding air implied an overestimation of the mean velocity of the gas phase at the edges of the jet ($r/X > 0.11$). The transverse mean velocity is most sensitive to the conditional seeding and can be overestimated up to 200% at the edges of the jet (Lehman, 1986).

In the present case, the flow being confined laterally, a small recirculation due to air entrainment brings oil droplets close to the edge of the jet. Therefore there is a clear difference of seeding between the jet and the surrounding air.

We proposed a method (Ferrand, 2001) to correct both the statistical bias due to the non-regular sampling of the tracers and the errors introduced by the conditional seeding.

This correction is based on the temporal reconstruction of the turbulent signal of the continuous phase. The statistics, which are now calculated from regularly sampled data, are not affected by the arrival time of the tracers in the measuring volume. In the same way these statistics are less sensitive to the non-homogeneous distribution of the tracers.

Radial profiles of the mean transverse velocity of the fluid "seen" by the drops ($\widetilde{V}_G$), calculated for four different size classes, can be found in (Ferrand, 2001). These radial profiles exhibit a maximum value located around $r/x = 0.1$. For the sake of brevity we will focus on this maximum value of $\widetilde{V}_G$ and V_G (the mean transverse velocity of the fluid), which contain basic information useful for the discussion. All the results are reported in Table 3.

The fluid velocity "seen" by the drops is clearly different from the gas velocity (last column in Table 3) and this gap is more pronounced for the small droplets (a factor 3 for the size class 5–10 μm). This property is linked with the non-homogeneous distribution of the drops injected only in the jet fluid. The small drops, responsive to the gas fluctuations (see Stokes numbers in Fig. 3) follow the turbulent structures of the jet. We therefore find them preferentially in the outgoing structures ($\widetilde{V}_G > V_G$), while the external fluid entrained by the jet contains no drop. This effect is all the more pronounced as the Stokes number of the drops is small. On the contrary, the drops of the class 80–90 μm, insensitive to most of gas fluctuations, are located indifferently in the outgoing

Table 3
Maximum value of the mean transverse velocity of the fluid seen by different drop size classes ($X = 20D_0$, $r/X \approx 0.08$)

Size class	5–10 μm	20–30 μm	50–60 μm	80–90 μm	Air (tracers corrected)
$(\widetilde{V}_G)_{max}$ (m s^{-1})	0.6	0.45	0.3	0.2	0.18

or re-entering turbulent structures. Thus, there is no correlation between the location of these drops and the gas velocity and the averaged velocity "seen" by the large drops should be equal to the local mean velocity of the carrier phase ($\widetilde{V}_G \approx V_G$). Table 3 shows that $\widetilde{V}_G$ tends toward V_G as D increases. This validates the statistical reconstruction of the fluid velocity "seen" by the particles presented here.

3.2. Results and discussion

3.2.1. Radial profile of the gas–droplet turbulent velocity correlations ($X = 20d_0$)

Once the fluid velocity "seen" by the drops is extracted from the temporal reconstruction of the gas phase velocity, it is then possible to calculate the gas–droplet turbulent correlations. First we present radial profiles ($X = 20d_0$) of the turbulent correlations for four different size classes and give some comments on the behaviour of these different correlations. Then, the results are exploited in the high shear zone of the jet in order to analyse the simplified form of the particle kinetic stress equation.

The radial profiles of the fluid–particle correlations $\langle u_G u_d \rangle_d$, $\langle v_G v_d \rangle_d$, $\langle u_G v_d \rangle_d$ and $\langle v_G u_d \rangle_d$ are plotted respectively in the Fig. 9a–d. From a general point of view, we observe that the droplets responsive to the turbulence of the fluid (see the longitudinal evolution of the Stokes number) present strong turbulent correlations with the continuous phase (close to the Reynolds stresses of the fluid), contrary to the big drops of stronger inertia. The longitudinal, radial and shear fluid/particles correlations $\langle u_G u_d \rangle_d$, $\langle v_G v_d \rangle_d$, $\langle v_G u_d \rangle_d$ and $\langle u_G v_d \rangle_d$ decrease when increasing the Stokes number.

Moreover one can note that the longitudinal and the shear turbulent correlations ($\langle u_G u_d \rangle_d$, $\langle u_G v_d \rangle_d$) are comparatively higher than the transverse turbulent correlations $\langle v_G v_d \rangle_d$. These properties are well highlighted by the Table 4 indicating the values of the turbulent correlations in the high shear zone of the jet (details concerning this region are given in the following section). One can note that the behaviour of the normalised coefficients $\langle u_G v_d \rangle_d / \langle u_G v_G \rangle$, $\langle u_G v_d \rangle_d / \langle u_G v_G \rangle$ and $\langle v_G u_d \rangle_d / \langle u_G v_G \rangle$ is strongly linked with the Stokes number: as soon as $St \approx O(1)$, these coefficients tend towards the unity. Table 3, Fig. 9c and d show also that the turbulent correlations $\langle v_G u_d \rangle_d$ are more sensitive to the turbulence of the fluid than $\langle u_G v_d \rangle_d$ so that $\langle v_G u_d \rangle_d$ are slightly higher than $\langle u_G v_d \rangle_d$ (Simonin et al., 1995). The fluid–particle correlation tensor is therefore non-symmetrical.

3.3. Particle kinetic stress equation: analysis in the high shear region of the jet and validation of the gas–droplet correlation measurements

The data relative to the dispersed phase, provided by the phase Doppler technique, lend themselves well to a physical analysis related to the Eulerian approach. In this approach, the dispersed phase is considered as a continuous field and transport equations of the volume fraction, the momentum and kinetic stresses are solved for each size-class, as for the gas phase. From now, the operator $\langle \cdot \rangle_d$ will denotes an average on the statistic properties of the size-class d.

According to the Eulerian model presented by Simonin et al. (1995), the kinetic stress equation of the dispersed phase ($\langle u_d u_d \rangle_d$, $\langle v_d v_d \rangle_d$, $\langle u_d v_d \rangle_d$) can be simplified in the shear region of the jet. The resulting equations provide simple relations between the kinetic stress of the drops and the tur-

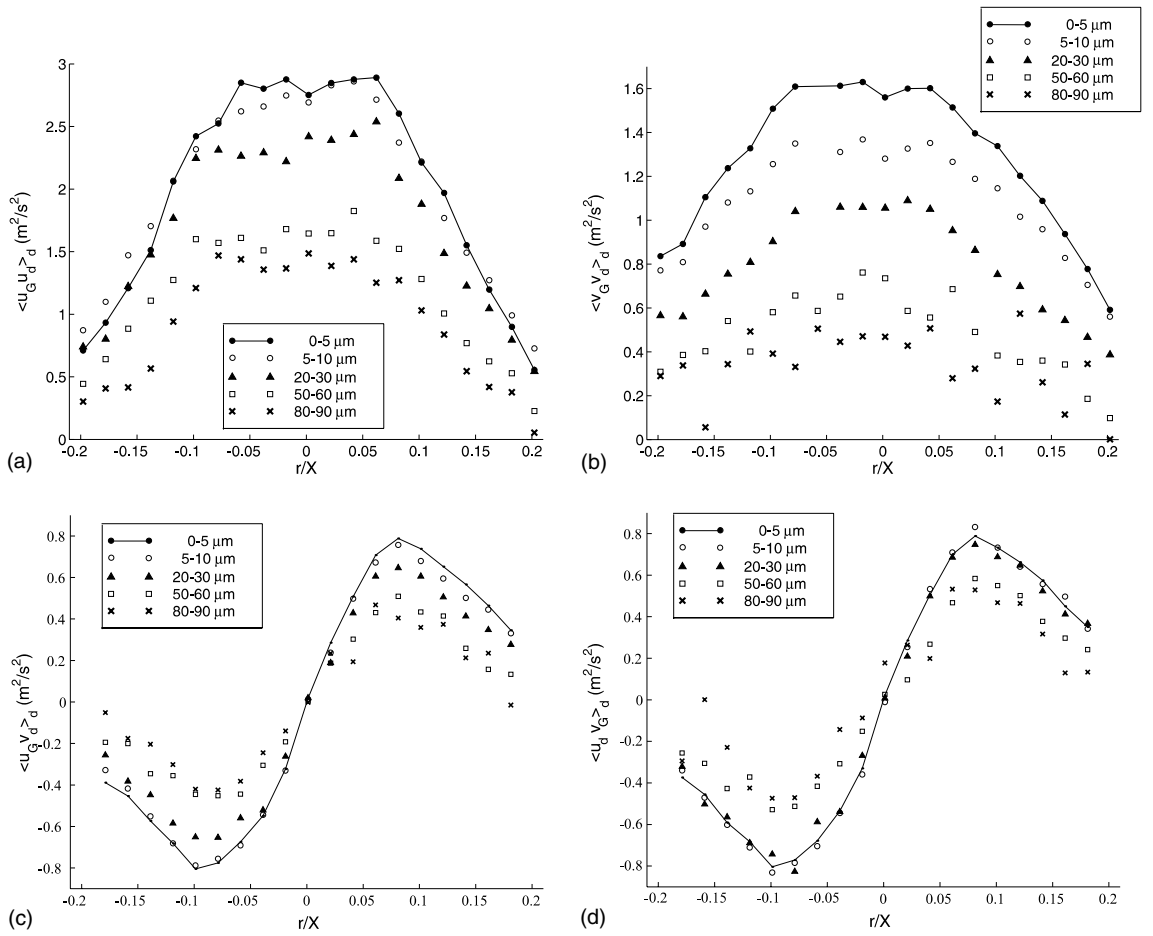

Fig. 9. Radial profiles of the gas–droplet turbulent velocity correlations for the different droplet size-classes, $X = 20d_0$: (a) longitudinal fluid–particle correlations $\langle u_G u_d \rangle_d$; (b) radial fluid–particle correlations $\langle v_G v_d \rangle_d$; (c) shear fluid–particle correlations $\langle u_G v_d \rangle_d$; (d) shear fluid–particle correlations $\langle v_G u_d \rangle_d$. Correlations of the size-class (0–5 μm) are corrected by the 'reconstruction' technique and correspond to the respective gas Reynolds stresses $\langle u_G u_G \rangle_G$, $\langle v_G v_G \rangle_G$ and $\langle u_G v_G \rangle_G$.

Table 4
Gas–droplet correlation coefficients according to the Stokes number, on the high shear region $r/X = 0.08$

Size class	5–10 μm	20–30 μm	50–60 μm	80–90 μm
Stokes number	0.012	0.51	2.10	3.30
$\langle u_G u_d \rangle_d / \langle u_G u_G \rangle$	1	0.91	0.63	0.54
$\langle v_G v_d \rangle_d / \langle v_G v_G \rangle$	0.93	0.72	0.46	0.22
$\langle u_G v_d \rangle_d / \langle u_G v_G \rangle$	1	0.86	0.61	0.57
$\langle v_G u_d \rangle_d / \langle u_G v_G \rangle$	1	0.99	0.7	0.64

bulent fluid/particle correlations. The simplifications of these equations are based on several assumptions. The objective of this section is to show that these assumptions are correctly validated

by the experimental results and that the measured turbulent fluid/particle correlations satisfy these equations.

The particle kinetic stress equation for discrete solid particles suspended in a turbulent flow can be found in Simonin et al. (1995). In a stationary axisymmetric particle laden jet, equations for $\langle u_d u_d \rangle_d$, $\langle v_d v_d \rangle_d$, read respectively:

$$U_d \frac{\partial \langle u_d u_d \rangle_d}{\partial X} + V_d \frac{\partial \langle u_d u_d \rangle_d}{\partial r} = -2\left(\langle u_d u_d \rangle_d \frac{\partial U_d}{\partial X} + \langle u_d v_d \rangle_d \frac{\partial U_d}{\partial r} \right) - \frac{1}{\alpha_d} \left(\frac{\partial \alpha_d \langle u_d u_d u_d \rangle_d}{\partial X} + \frac{\partial r \alpha_d \langle u_d u_d v_d \rangle_d}{r \partial r} \right) - \frac{2}{\tau_d} (\langle u_d u_d \rangle_d - \langle u_G u_d \rangle_d) \tag{3.1}$$

$$U_d \frac{\partial \langle v_d v_d \rangle_d}{\partial X} + V_d \frac{\partial \langle v_d v_d \rangle_d}{\partial r} = -2\left(\langle u_d v_d \rangle_d \frac{\partial V_d}{\partial X} + \langle v_d v_d \rangle_d \frac{\partial V_d}{\partial r} \right) - \frac{1}{\alpha_d} \left(\frac{\partial \alpha_d \langle u_d v_d v_d \rangle_d}{\partial X} + \frac{\partial r \alpha_d \langle v_d v_d v_d \rangle_d}{r \partial r} - \frac{2 \alpha_d \langle v_d w_d w_d \rangle_d}{r} \right) - \frac{2}{\tau_d} (\langle v_d v_d \rangle_d - \langle v_G v_d \rangle_d) \tag{3.2}$$

The first term on the right-hand side of (3.1) and (3.2) represents the production from the particle mean velocity gradient. The second term is the transport of kinetic stress by the particle velocity fluctuations. The third term is an approximate form of the turbulent momentum transfer rate from the fluid turbulent motion. The first part of this contribution, proportional to the particle kinetic stress $\langle u_d u_d \rangle_d$ and $\langle v_d v_d \rangle_d$, respectively, is a sink term due to the drag force. Conversely, the second part of this contribution, proportional to the fluid-particle turbulent correlation $\langle u_G u_d \rangle_d$ and $\langle v_G v_d \rangle_d$, respectively is a source term representing the dragging of the particle by the fluid turbulence.

Using the classical boundary layer assumption and experimental observations on statistics of the radial particle velocity, Simonin et al. (1995) and Prévost et al. (1996) demonstrated that Eq. (3.2) can be significantly simplified and reads:

$$\langle v_d v_d \rangle_d \approx \langle v_G v_d \rangle_d \tag{3.3}$$

Eq. (3.3) indicate that the dragging of the particles by the fluid turbulence controls the transverse kinetic stresses of the particles.

The measured quantities in the high shear region ($r/X = 0.08$) of the profile $X = 20 d_0$ are shown in Fig. 10a. The expected statistical error bars are reported on the graphs. Fig. 10a indicates the behaviour of the radial droplet kinetic stress $\langle v_d v_d \rangle_d$ versus droplet sizes. Its value remains smaller than the corresponding fluid Reynolds stress $\langle v_G v_G \rangle$ and decreases progressively as the droplet diameter increases. One can observe, moreover, that the measured radial kinetic stress $\langle v_d v_d \rangle_d$ lies very close to the measured transversal gas–droplet correlation $\langle v_G v_d \rangle_d$, in accordance with the simplified Eq. (3.3).

Eq. (3.1) cannot be so easily simplified as transport and production term are not negligible all over the radial profile of the jet. Nevertheless, one can show that the production term is dominant in the high shear region (Hussein et al., 1994). In that region, the longitudinal kinetic stress equation (3.1) can be simplified in Simonin et al. (1995):

$$\langle u_d u_d \rangle_d \approx \langle u_G u_d \rangle_d - \tau_d \langle u_d v_d \rangle_d \frac{\partial U_d}{\partial r} \tag{3.4}$$

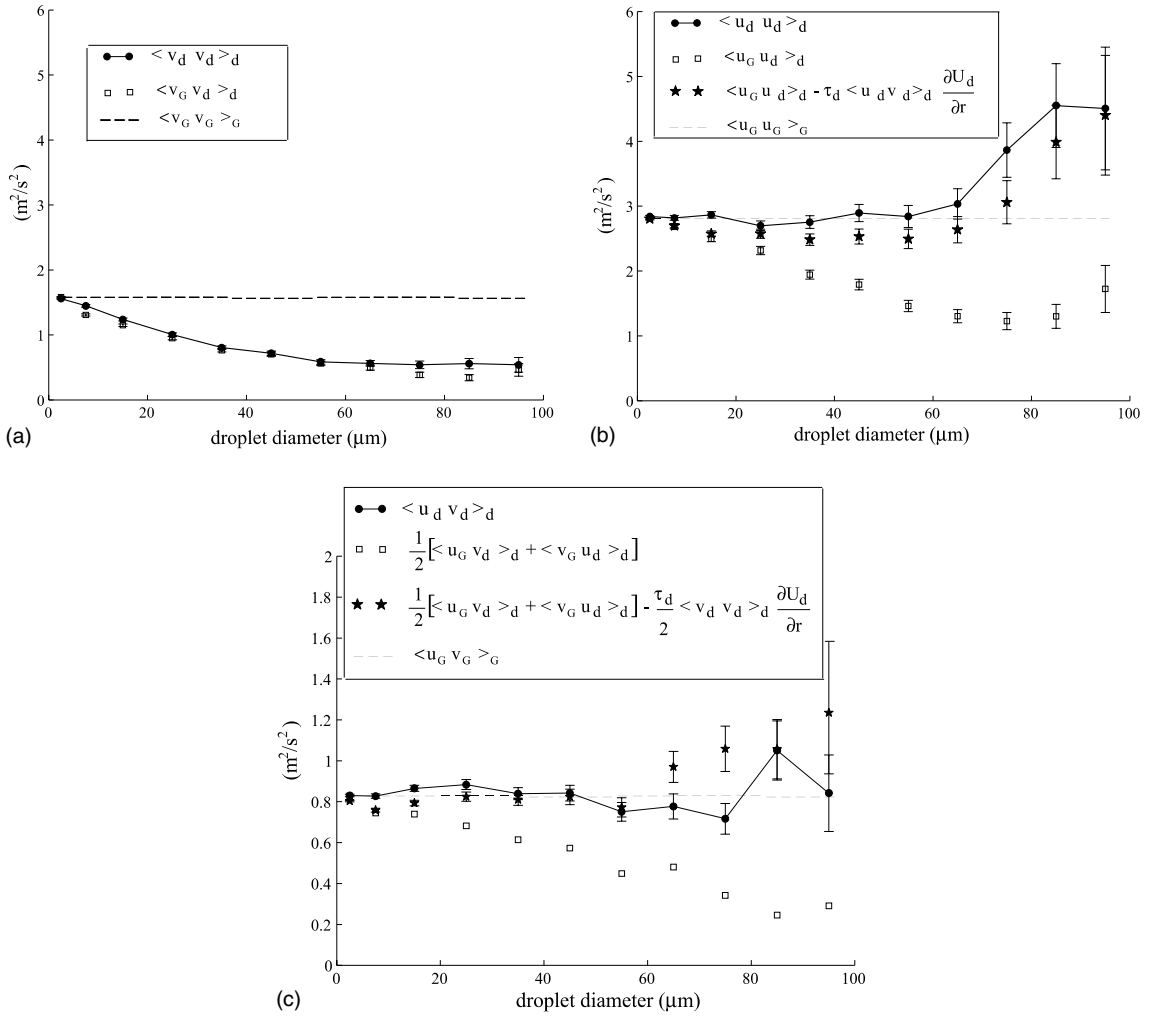

Fig. 10. Evolution of the droplets kinetic and shear stresses and the corresponding gas–droplet correlations according to the droplet size. Validation of the simplified Eqs. (a) (3.3), (b) (3.4) and (c) (3.5) in the high shear region ($r/X = 0.08$) of the jet, $X = 20d_0$.

Fig. 10b represents the evolution of the longitudinal droplet kinetic stress $\langle u_d u_d \rangle_d$ for the different size classes. It is observed, in contrast to the transverse fluctuations, that $\langle u_d u_d \rangle_d$ remains equivalent to the corresponding fluid Reynolds stress $\langle u_G u_G \rangle$ for droplet diameters smaller than 50 μm ($St \ll 1$ or $St = O(1)$) and grows for the larger size classes ($St \gg 1$).

We saw (Fig. 9a) that the correlations $\langle u_G u_d \rangle_d$ decrease continuously when the droplet size increases. Therefore, the difference between the longitudinal droplet kinetic stress $\langle u_d u_d \rangle_d$ and the corresponding gas–droplet correlation $\langle u_G u_d \rangle_d$ increases as droplet size increases. Following Eq. (3.4), this difference is expected to be due to the mean gradient production term $(-\tau_d \langle u_d v_d \rangle_d \partial U_d / \partial r)$. One can observe that the experimental measurements are in good agreement with that prediction. In the high shear region of the jet, the production of the longitudinal kinetic

stress by the mean particle velocity gradient is then the main contributor to the difference between $\langle u_d u_d \rangle_d$ and $\langle u_G u_d \rangle_d$. This production term, absent from the radial droplet kinetic stress $\langle v_d v_d \rangle_d$ determination, is the source of the strong anisotropy observed for the droplet fluctuating motion in such shear flows (Hishida et al., 1992; Février and Simonin, 1998).

As phase Doppler measurements are performed with a two-component laser, information are also available for the droplet shear stress $\langle u_d v_d \rangle_d$. Using a comparable simplification than for Eq. (3.4), valid for a stationary high shear flow, the particle shear stress equation can also be written:

$$\langle u_d v_d \rangle_d \approx \frac{1}{2}(\langle u_G v_d \rangle_d + \langle v_G u_d \rangle_d) - \frac{\tau_d}{2}\langle v_d v_d \rangle_d \frac{\partial U_d}{\partial r} \tag{3.5}$$

However one can observe in Fig. 10c that the droplet shear stress $\langle u_d v_d \rangle_d$ estimated from the gas–droplet correlations ($\langle u_G v_d \rangle_d$ and $\langle v_G u_d \rangle_d$) and the production term (Eq. (3.5)) overestimates the magnitude of $\langle u_d v_d \rangle_d$ for large particle classes ($D < 50$ μm).

Fig. 10a–c provide a satisfactory validation both for the phase Doppler measurements and for the post processing of the data: temporal reconstruction of the turbulent signal, correction of the bias due to the conditional seeding and extraction of the fluid velocity "seen" by the particles. Moreover these experimental measurements confirm the assumptions used to write the simplified form of the particle normal stresses equations in the high shear region of the jet.

4. Contribution of the fluid–particle correlations on the turbulent interaction between phases

This section is dedicated to the attenuation term, Π, which complements the classical expression of the transport equations for single-phase flows (see Eqs. (1.1)–(1.3)). More precisely the objective is to provide the radial evolution ($X = 20d_0$) of the terms $\Pi_{G_{\langle uu \rangle}}$, $\Pi_{G_{\langle vv \rangle}}$ and $\Pi_{G_{\langle uv \rangle}}$, and to estimate the weight of the fluid–particle correlations on the "direct" turbulent interaction between the particles and the surrounding fluid.

Following the Eulerian approach proposed by Simonin et al. (1995), the direct interaction terms between the fluctuating flow of the gas phase and the drops of a given size class d, are written as:

$$\Pi_{G_{\langle uu \rangle d}} = -\frac{\alpha_d \rho_L}{\rho_G}\frac{2}{\tau_d}[\langle u_G u_G \rangle_d - \langle u_G u_d \rangle_d - \langle u_G \rangle_d \langle U_G - U_d \rangle_d] \tag{4.1}$$

$$\Pi_{G_{\langle vv \rangle d}} = -\frac{\alpha_d \rho_L}{\rho_G}\frac{2}{\tau_d}[\langle v_G v_G \rangle_d - \langle v_G v_d \rangle_d - \langle v_G \rangle_d \langle V_G - V_d \rangle_d] \tag{4.2}$$

$$\begin{aligned}\Pi_{G_{\langle uv \rangle d}} = -\frac{\alpha_d \rho_L}{\rho_G}\frac{1}{\tau_d}[&2\langle u_G v_G \rangle_d - (\langle u_G v_d \rangle_d + \langle v_G u_d \rangle_d) \\ &- (\langle u_G \rangle_d \langle V_G - V_d \rangle_d + \langle v_G \rangle_d \langle U_G - U_d \rangle_d)]\end{aligned} \tag{4.3}$$

One can note the competitive roles played by the drop time constant (τ_d) and the local concentration of its size class ($\langle Cm_d \rangle = \alpha_d \rho_L$): the drop distribution used in our configuration implies that $\langle Cm_d \rangle$ decreases (see Fig. 4) whereas $1/\tau_d$ increases when the size class decreases.

The terms between brackets (for instance in Eq. (4.1)) correspond respectively to the Reynolds stress of the fluid "seen" by the particles, $\langle u_G u_G \rangle_d$ and to the turbulent correlations between the

velocity of the drops and the continuous phase $\langle u_G u_d \rangle_d$. The term $\langle u_G \rangle_d \langle U_G - U_d \rangle_d$, relative to the exchange with the mean flow, can be neglected in our configuration (Ferrand, 2001).

Owing to the temporal reconstruction of the fluid velocity we verified (Ferrand, 2001) that the Reynolds stress of the fluid "seen" by the particles can be correctly approximated by the "classical" fluid Reynolds stress ($\langle u_{G,i} u_{G,j} \rangle_d \approx \langle u_{G,i} u_{G,j} \rangle$), as generally assumed in the models (Simonin et al. (1995)).

Since the fluid–particle correlations are lower than the corresponding fluid Reynolds stress (Section 3), $\Pi_{G_{\langle uu \rangle d}}$, $\Pi_{G_{\langle vv \rangle d}}$ and $\Pi_{G_{\langle uv \rangle d}}$ are negative terms that contribute to a decrease in the turbulence intensity of the continuous phase. This observation is consistent with the expected behaviour of the drops present in the jet, insofar as their size is low compared to the integral scales of turbulence, and their Reynolds numbers remain always small ($Re_p < 100$) (Hetsroni, 1989; Gore and Crowe, 1989).

For each size class, the results concerning the local liquid mass fraction and the fluid–particle correlations have been gathered to calculate the terms of direct interaction between phases. Radial profiles of $\Pi_{G_{\langle uu \rangle}}$, $\Pi_{G_{\langle vv \rangle}}$ and $\Pi_{G_{\langle uv \rangle}}$ are presented in Fig. 11a–c respectively, after summing on all the size classes.

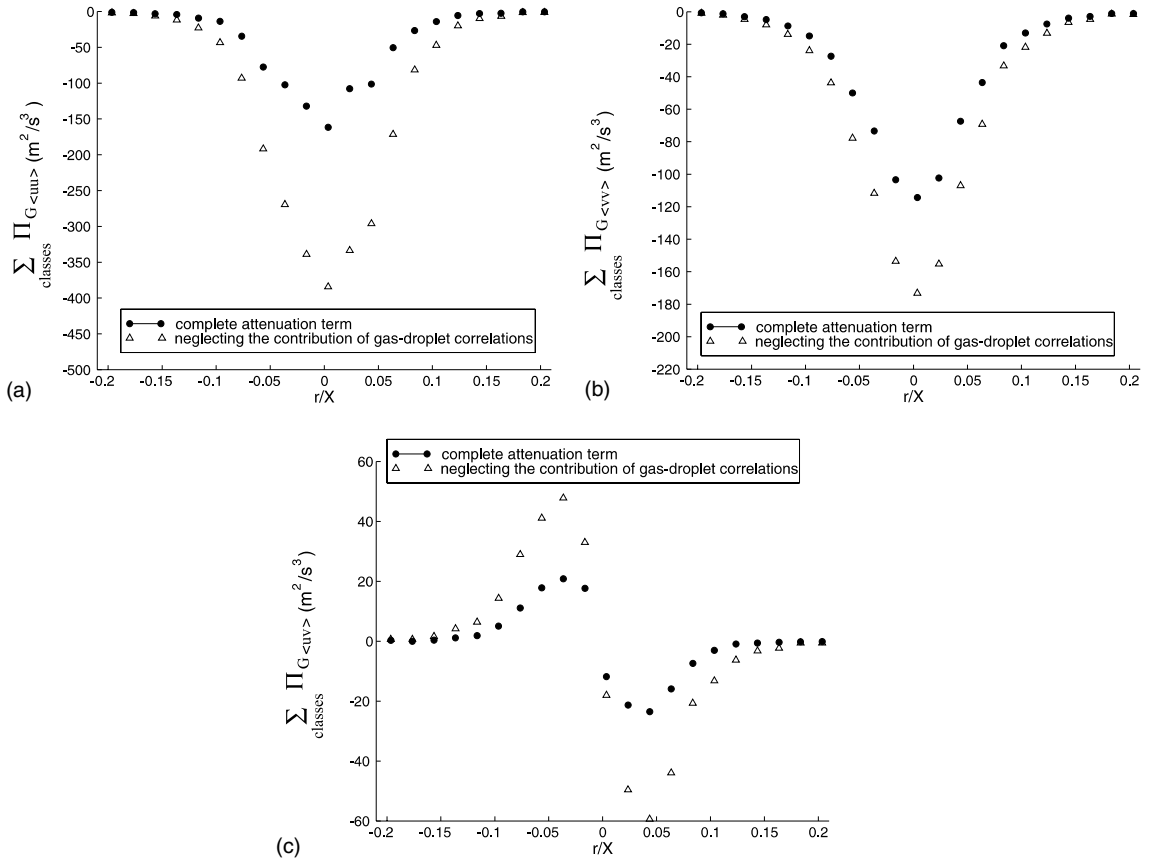

Fig. 11. (a–c) Radial profile of the turbulent attenuation terms $\sum_{classes} \Pi_{G_{\langle uu \rangle}}$, $\sum_{classes} \Pi_{G_{\langle vv \rangle}}$ and $\sum_{classes} \Pi_{G_{\langle uv \rangle}}$ ($X = 20 d_0$). Comparison with the estimation obtained when neglecting the contribution of gas–droplet correlation.

The attenuation terms $\Pi_{G_{\langle uu\rangle}}$, $\Pi_{G_{\langle vv\rangle}}$ play an important role near the jet centreline where the liquid concentration reaches a maximum value (see Fig. 4), whereas $\Pi_{G_{\langle uv\rangle}}$ is maximum in the high shear regions of the jet. To check that Π is significant when compared to the production term, the ratio $(\Pi_{G\langle uu\rangle})_{max}/(P_{G\langle uu\rangle})_{max}$ has been calculated on the radial profile (Ferrand, 2001) and reaches a maximum value of 20%. This value is quite moderate because of the decrease in liquid concentration at this axial location, but its proves that direct interaction with turbulence has to be taken into in the models, especially for a correct prediction of the dense regions of such a two-phase flow.

To be more complete, we compare these radial profiles of Π with the estimation of the attenuation terms usually found in the literature, when neglecting the fluid–particle correlations in Eqs. (4.1)–(4.3). The graphs, superimposed in the Fig. 11a–c, clearly show that these estimations really overestimate the magnitude of the attenuation terms (respectively by a factor 2.5, 1.6 and 3 for $\Pi_{G_{\langle uu\rangle}}$, $\Pi_{G_{\langle vv\rangle}}$ and $\Pi_{G_{\langle uv\rangle}}$). Following this assumption, a ratio $(\Pi_{G\langle uu\rangle})_{max}/(P_{G\langle uu\rangle})_{max}$ of approximately 50% would be predicted here for example. Any prediction based on such hypothesis would therefore strongly fail.

Hence, these results demonstrate experimentally that one key point for the prediction of turbulence attenuation by droplets is the prediction of gas–droplet correlations.

5. Concluding remarks

Analysis of gas–droplet turbulent velocity correlations and two-phase interaction in an axisymmetric jet were presented in this paper. The experimental configuration is a turbulent, droplet-laden jet, where the initial liquid mass loading (73%) is large enough to modify the mean and fluctuating velocity fields of the carrier phase. This effect, referred as "two-way coupling", has been clearly observed and the turbulence attenuation by the dispersed phase was quantified (−19% for the centreline turbulent kinetic energy at 20 diameters from the jet exit).

Statistics of the fluid velocity seen by the particle are particularly important in understanding fluid–particle interaction. They have been determined owing the temporal reconstruction of the gas phase velocity provided by phase Doppler data. This method was applied at 20 diameters from the jet exit. Since the particle diameters cover a wide range, various behaviours have been observed from the droplets that perfectly follow the fluid ($St \ll 1$) to those non-responsive to most of gas fluctuations ($St \gg 1$). The preferential association of the responsive particles with the outgoing structures of the jet has been well detected: the mean transverse velocity of the continuous phase seen by the smallest droplets is locally 300% higher than the mean transverse velocity of the fluid. On the contrary, the mean lateral velocity of the non-responsive particles is close to the unbiased gas velocity. This result was expected and is a validation of the measurement procedure.

Following an Eulerian approach presented by Simonin et al. (1995), the equations governing the particle kinetic stresses were written. They can be simplified in the high shear region of the jet and the resulting equations provide simple relations between the kinetic stresses of the drops and the turbulent fluid/particle correlations. Our measurements are in good agreements with the predicted trends. The radial droplet kinetic stress $\langle v_d v_d\rangle_d$ decreases progressively as the droplet diameter increases. $\langle v_d v_d\rangle_d$ lies very close to the measured transversal gas–droplet correlation

$\langle v_G v_d \rangle_d$. The radial droplet kinetic stress is thus mainly controlled by dragging from fluid turbulence. In contrast to the transverse fluctuations, the longitudinal correlation $\langle u_d u_d \rangle_d$ remains equivalent to the corresponding fluid Reynolds stress $\langle u_G u_G \rangle$ for droplet diameters smaller than 50 μm and grows for the larger size classes. On the other hand the correlations $\langle u_G u_d \rangle_d$ decrease continuously when the droplet size increases. Therefore, the difference between $\langle u_d u_d \rangle_d$ and $\langle u_G u_d \rangle_d$ increases with the droplet size. According to the theory, we showed that this difference is mainly du to the production of longitudinal kinetic stress by the mean particle velocity gradient. This production term, absent from the radial droplet kinetic stress $\langle v_d v_d \rangle_d$, is the source of the strong anisotropy observed for the droplet fluctuating motion in such shear flows.

The terms $\Pi_{G,ij}$, relative to the turbulent kinetic energy transfer from the particles to the gas, have been calculated for the radial profile $X = 20d_0$. Such results require both the knowledge of the fluid–particle correlations and the local concentration of the liquid phase per size class (these data were provided owing a coupling method (Ferrand et al., 2001) between the phase Doppler technique and laser induced fluorescence). $\Pi_{G_{\langle uu \rangle}}$ and $\Pi_{G_{\langle vv \rangle}}$ are negative terms that contribute to a decrease in the turbulence intensity of the continuous phase. The direct attenuation is proportionally more pronounced for the transversal component and this anisotropy is probably linked to the fact that the fluid–particle correlations are less important in that direction. $\Pi_{G_{\langle uv \rangle}}$ is maximum in the high shear region of the jet. This result confirms the marked effects of the direct interaction between phases on the shear Reynolds stress and afterwards on the radial turbulent diffusion.

Finally, for the first time to our knowledge, the weight of the fluid–particle correlations on the direct turbulent interaction between phases has been evaluated experimentally. Neglecting the fluid–particle correlated motion leads to overestimate the magnitude of the attenuation terms (respectively by a factor 2.5, 1.6 and 3 for $\Pi_{G_{\langle uu \rangle}}$, $\Pi_{G_{\langle vv \rangle}}$ and $\Pi_{G_{\langle uv \rangle}}$). Hence, these results demonstrate that one key point for the prediction of turbulence attenuation by droplets is the prediction of gas–droplet correlations.

Acknowledgements

The authors wish to acknowledge financial support from Renault, Siemens Automotive and the Centre National de la Recherche Scientique (CNRS). The authors would also like to thank Prof. O. Simonin for fruitful discussions. G. Couteau and E. Cid are greatly acknowledged for technical support.

References

Berlemont, A., Simonin, O., Sommerfeld, M., 1995. Validation of inter-particle collision models based on large eddy simulation. Proceedings ASME Symposium on Gas Solid Flows.

Borée, J., Ishima, T., Flour, I., 2001. The effect of mass loading and inter-particle collisions on the development of polydispersed two-phase flow downstream a confined bluff-body. J. Fluid Mech 443, 129–165.

Crowe, C.T., 2000. On models for turbulence modulation in fluid–particle flows. Int. J. Multiphase Flow 26, 719–727.

Elghobashi, S.E., Abou-Arab, T.W., 1983. A two-equation turbulence model for two-phase flows. Phys. Fluid 26, 169–209.

Ferrand, V., Bazile, R., Borée, J., 2001. Measurements of concentration per size class in a dense polydispersed jet using planar laser-induced fluorescence and phase Doppler techniques. Exp. Fluids 31, 597–607.

Ferrand, V., 2001. Analyse physique d'un jet d'air turbulent chargé en gouttelettes. Diagnostics laser applicables à l'injection directe dans les moteurs. Ph.D. Thesis I.N.P. Toulouse, France.

Février, P., Simonin, O., 1998. Constitutive relations for fluid–particle velocity correlations in gas–solid turbulent flows. In: Proceedings of Third International Conference on Multiphase Flow.

Fleckhauss, D., Hishida, K., Maeda, M., 1987. Effects of laden solid particles on the turbulent flow structure of a round free jet. Exp. Fluids 5, 323–333.

Gore, R.A., Crowe, C.T., 1989. Effect of particle size on modulating turbulent intensity. Int. J. Multiphase Flow 15, 279–285.

Hädrich, T.H., Erdmann, H.J., 1998. Measurement of particle–fluid velocity correlation on dispersed gas–solid flows. In: Proceedings of Third International Conference on Multiphase Flow.

Hardalupas, Y., Taylor, A.M.K.P., Whitelaw, J.H., 1989. Velocity and particle-flux characteristics of turbulent particle-laden jets. In: Proceedings of Royal Society of London, pp. 31–78.

Hetsroni, G., 1989. Particles-turbulence interaction. Int. J. Multiphase Flow 15, 735–746.

Hinze, J.O., 1975. Turbulence. In: Mc-Graw-Hill series in mechanical engineering. Kingsport Press.

Hishida, K., Ando, A., Maeda, A., 1992. Experiments on particle dispersion in a turbulent mixing layer. Int. J. Multiphase Flow 18, 181–194.

Hussein, H.J., Capp, S.P., George, W.K., 1994. Velocity measurements in a high-Reynolds-number, momentum-conserving, axisymmetric, turbulent jet. J. Fluid Mech. 258, 31–75.

Kenning, V.M., Crowe, C.T., 1997. On the effect of particles on carrier phase turbulence in gas–particle flows. Int. J. Multiphase Flow 23, 403–408.

Kulick, J.D., Fessler, R., Eaton, J.K., 1994. Particle response and turbulence modification in fully developed channel flow. J. Fluid Mech. 277, 109–134.

Lehman, B., 1986. Laser-Doppler-Messungen in einem turbulenten Freistrahl. DFVLR-Forschungsbericht.

Longmire, E.K., Eaton, J.K., 1992. Structure of a particle-laden round jet. J. Fluid Mech. 236, 217–257.

Longmire, H.K., Khalitov, D.A., Anderson, S.L., Borée, J., 1999. Planar field velocity measurements in gas–solid flows. In: Proceedings of Third ASME/JSME Joint Fluid Engineering Conference.

Modaress, D., Tan, H., Elghobashi, S., 1983. Two component LDA measurements in a two-phase turbulent jet. AIAA J. 2, 624–630.

Mostafa, A.A., Mongia, H.C., 1988. On the interaction of particles and turbulent fluid flow. Int. J. Heat Mass Transfer 31, 2063–2075.

Parthasarathy, R.N., Faeth, G.M., 1990. Turbulence modulation in homogeneous dilute particle-laden flows. J. Fluid Mech. 220, 485–514.

Petrie, H.L., Samimy, M., Addy, A.L., 1988. Laser-Doppler velocity bias in separated turbulent flows. Exp. Fluids 6, 80–88.

Prévost, F., Borée, J., Nuglish, H.J., Charnay, G., 1996. Measurements of fluid/particle correlated motion in the far field of an axisymmetric jet. Int. J. Multiphase Flow 22, 685–701.

Qiu, H.H., Sommerfeld, M., 1992. A reliable method for determining the measurement volume size and particle mass fluxes using phase-Doppler anemometry. Exp. Fluids 13, 393–404.

Sakakibara, J., Wicker, R.B., Eaton, J.K., 1996. Measurements of particle–fluid velocity correlation and extra dissipation in a round jet. Int. J. Multiphase Flow 22, 863–881.

Sautet, C., 1992. Effets des differences de densité sur le developpement scalaire et dynamique des jets turbulents. Ph.D. Thesis, Rouen university, France.

Simonin, O., 1991. Prediction of the dispersed phase turbulence in particle-laden jets. In: Proceedings of the Fourth International Symposium On Gas–Solid Flows, ASME FED, vol. 121, pp. 197–206.

Simonin, O., 2000. Theoretical and experimental modeling of particulate flow. Lecture Series 2000-06, Von Karman Institute for Fluid Dynamics.

Simonin, O., Deutch, E., Boivin, M., 1995. Large eddy simulation and second moment closure model of particle fluctuating motion in two-phase turbulent shear flows. In: Proceedings of the Ninth International Symposium on Turbulent Shear Flows.

Sommerfeld, M., 1993. Review of numerical modelling of dispersed two-phase flows. Fifth International Symposium on refined flow modelling and turbulence measurements, Paris.

Squires, K.D., Eaton, J.K., 1990. Particle response and turbulence modification in isotropic turbulence. Phys. Fluids A 2, 1191–1203.

Veynante, D., Candel, S.M., 1988. Application of non linear spectral analysis and signal reconstruction to laser Doppler velocimetry. Exp. Fluids 6, 534–540.

Wygnanski, I., Fielder, H., 1969. Some measurements in the self preserving jet. J. Fluid Mech. 38, 577–612.

Yarin, L.P., Hetsroni, G., 1994. Turbulence intensity in dilute two-phase flows. Int. J. Multiphase Flow 20, 27–44.

Yuan, Z., Michaelides, E.E., 1992. Turbulence modulation in particulate flows—A theoretical approach. Int. J. Multiphase Flow 18, 779–785.